Two CMOS Dual-Feedback Common-Gate Low-Noise Amplifiers With Wideband Input and Noise Matching

Rong-Fu Ye, *Student Member, IEEE*, Tzyy-Sheng Horng, *Senior Member, IEEE*, and Jian-Ming Wu, *Member, IEEE*

***Abstract*—This paper presents two CMOS common-gate (CG) low-noise amplifiers (LNAs) using different dual-feedback techniques, significantly reducing noise figure (NF) to around 2 dB over a wide frequency range. The proposed first CG LNA uses g_m-boosted feedback and shunt-series transformer feedback to relieve the tradeoff between input and noise matching. The proposed second CG LNA further extends the input matching bandwidth by using g_m-boosted feedback and shunt–shunt transformer feedback. Moreover, the transformer used for feedback in both CG LNAs causes gain peaking and thus a considerable increase of 3-dB gain bandwidth. After implementation in a 0.18-μm CMOS process, the first and second CG LNAs achieve an NF of 1.9–2.6 dB over a 3-dB gain bandwidth of 7 and 10 GHz, respectively. The comparison between simulated and measured results shows a good agreement.**

***Index Terms*—CMOS low-noise amplifier (LNA), common-gate (CG) LNA, dual feedback, wideband LNA.**

I. Introduction

THE increasingly pervasive use of wireless broadband technology is due to its high data-rate transmission capability. For future wireless communication systems, a universal software-defined radio (SDR) provides a tunable platform over a wide frequency range, which covers multiple wireless communication standards, including a multi-band/ multi-standard system ranging from 1 to 6 GHz and an ultra-wideband (UWB) system ranging from 3.1 to 10.6 GHz. To achieve an RF receiver operating within a spectrum of both multi-band/multi-standard and UWB systems, a wideband receiver is more efficient and flexible in terms of power consumption, chip area, and cost than the parallel multiple narrowband receivers for high-level integration in a single chip [1], [2]. Despite the advantage of a wideband receiver having hardware shared with multi-standards, this feature poses a more stringent requirement on the wideband receiver. As a critical block in a wideband receiver, a low-noise amplifier (LNA) must provide adequate input matching, high linearity, low noise figure (NF), and sufficient gain over a wide frequency range to obtain a high dynamic range for a wideband receiver with low power consumption [3], [4].

Common-gate (CG) amplifiers are generally promising for use in wideband due to their high stability, linearity, and reverse isolation [5], [6]. However, because of the difficulty in wideband noise matching, their NF performance is poorer than that of common-source (CS) amplifiers. Additionally, the 3-dB gain bandwidth of CG LNA is rather finite unless using the gain peaking technique [7]. Cascaded topologies usually consume large dc currents [8]–[10]. The CG LNA that uses the parallel noise-canceling technique to suppress the channel thermal noise of a MOSFET can reduce NF to 3–4 dB [11]–[13]; however, it excessively counts on the balance of output amplitude and phase. Moreover, the negative feedback [14], [15] or positive feedback [16], [17] technique can reduce the NF of the CG LNA to an average of 3 dB. However, due to the limited feedback gain, further improvement is rather difficult. To improve the NF, the use of a dual (positive and negative) feedback technique can further reduce the NF of the CG LNA to around 2 dB [18]. Nonetheless, its 3-dB gain bandwidth is restricted by the output RC time constant.

This paper presents two CMOS dual-feedback CG LNAs using g_m-boosted and transformer feedback to achieve a low NF and a flat power gain over a wide band of frequencies. The first CG LNA (referred to as CG LNA-1) uses the topology of shunt–shunt negative feedback and shunt-series positive feedback to relieve the tradeoff between input and noise matching [19]. This paper extends the previous work [19] by performing the output series peaking via transformer to increase the 3-dB gain bandwidth. Although the CG LNA-1 has a superior NF and 3-dB gain bandwidth, its applicable frequency range is not wide enough to cover 3.1–10.6 GHz for UWB applications. Therefore, the second CG LNA (referred to as CG LNA-2) uses shunt–shunt negative feedback, shunt–shunt positive feedback, and output shunt-series peaking to achieve a similar NF, but a much wider 3-dB gain bandwidth than the CG LNA-1 for meeting the need of an UWB LNA design.

II. Circuit Analysis

A. Differential CG LNA With a g_m-Boosted Feedback

Fig. 1(a) illustrates a half circuit of the conventional CG LNA (referred to as CG LNA-gb) using a g_m-boosted feedback as

Manuscript received February 09, 2013; revised July 22, 2013; accepted July 25, 2013. Date of publication August 19, 2013; date of current version October 02, 2013. This work was supported in part by the National Science Council, Taiwan under Grant 101-2622-E-110-005-CC3, Grant 100-2221-E-110-081-MY3, and Grant 100-2221-E-110-082-MY3.

R.-F. Ye and T.-S. Horng are with the Department of Electrical Engineering, National Sun Yat-Sen University, Kaohsiung 80424, Taiwan (e-mail: d963010022@student.nsysu.edu.tw; jason@ee.nsysu.edu.tw).

J.-M. Wu is with the Department of Electronic Engineering, National Kaohsiung Normal University, Kaohsiung 82424, Taiwan (e-mail: jianmingwu@nknu.edu.tw).

Color versions of one or more of the figures in this paper are available online at http://ieeexplore.ieee.org.

Digital Object Identifier 10.1109/TMTT.2013.2277997

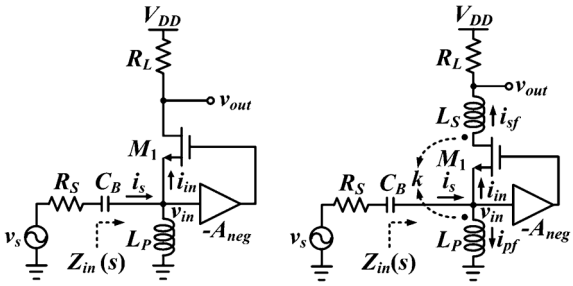

Fig. 1. Half circuits of the differential CG LNAs. (a) CG LNA-gb. (b) CG LNA-1.

a shunt–shunt negative feedback [14]. The input impedance of CG LNA-gb is derived as

$$Z_{\rm in}(s) = \frac{v_{\rm in}(s)}{i_s(s)} = \left[g_m(1 + A_{\rm neg}) + sC_{\rm gs} + \frac{1}{sL_P} \right]^{-1} \quad (1)$$

where g_m, L_P, and $C_{\rm gs}$ are the transconductance of transistor M_1, source inductance of M_1, and gate-to-source capacitance of M_1, respectively. $A_{\rm neg}$ denotes an inverting feedback loop gain. Clearly, the negative feedback boosts the g_m value by a factor of $(1+A_{\rm neg})$. From (1), $Z_{\rm in}(s)$ is approximated as $1/g_m(1+A_{\rm neg})$ when L_P resonates with $C_{\rm gs}$. For input matching, $g_m(1+A_{\rm neg})$ should be set equal to the terminating source conductance $G_S = 1/R_S = 20$ mS, where R_S is the terminating source resistance. Additionally, the dominant noise sources are assumed here to be channel thermal noise of M_1 and thermal noise of output load resistance R_L. Therefore, the noise factor F of the CG LNA-gb under input matching is derived as

$$F = 1 + \frac{\gamma}{\alpha} \frac{1}{(1 + A_{\rm neg})} + \frac{4R_S}{R_L} \quad (2)$$

where γ and α are the thermal noise coefficient of the transistor and ratio of g_m to zero-bias drain conductance, respectively. The value of γ/α is generally equal to 1.33 for short-channel MOSFETs [20]. From (2), the negative feedback obviously reduces the noise contribution from M_1 by a factor of $(1+A_{\rm neg})$. Additionally, the frequency-dependent voltage gain of CG LNA-gb is derived as

$$A_v(s) = \frac{v_{\rm out}(s)}{v_{\rm in}(s)} = \frac{R_L}{Z_{\rm in}(s)(1 + sC_{\rm out}R_L)} \quad (3)$$

where $C_{\rm out}$ is the output capacitance of M_1, which includes the drain capacitance C_d of M_1 and the input capacitance C_n of the subsequent stage. According to (2) and (3), the R_L value should be as large as possible to reduce the NF, and meanwhile increase the voltage gain. However, an excessively large R_L significantly degrades the 3-dB gain bandwidth, which is expressed as $1/R_LC_{\rm out}$. Based on the above discussion, we can infer that g_m is restricted stringently by input matching. Consequently, R_L becomes the dominant factor to determine NF and voltage gain, which is a tradeoff with the 3-dB gain bandwidth and linearity.

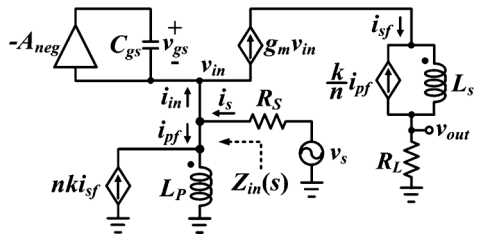

Fig. 2. Small-signal equivalent half circuit of the proposed CG LNA-1.

B. Differential CG LNA With a g_m-Boosted and Shunt-Series Dual Feedback

Fig. 1(b) illustrates a half circuit of the proposed CG LNA-1 [19]. The dual-feedback structure comprises a g_m-boosted feedback as a shunt–shunt negative feedback and a transformer feedback as a shunt-series positive feedback. The transformer, which consists of primary winding inductance L_P and secondary winding inductance L_S, makes the current gain of CG LNA-1 larger than one. Moreover, in addition to consuming no dc power, the loop gain of the positive feedback is a product of the magnetic coupling coefficient and a turn ratio of the transformer, thereby making the positive feedback independent of process, voltage, and temperature (PVT) variations.

1) Input Impedance: Fig. 2 illustrates the small-signal equivalent half circuit of CG LNA-1, which ignores the channel length modulation of M_1. The $Z_{\rm in}(s)$ of CG LNA-1 is found as

$$Z_{\rm in}(s) = \left[g_m(1 + A_{\rm neg})(1 - n \cdot k) + sC_{\rm gs} + \frac{1}{sL_P} \right]^{-1} \quad (4)$$

where k is the coefficient of magnetic coupling and $n = \sqrt{L_S/L_P}$ is the turn ratio of the transformer. In contrast with (1), (4) indicates that $n \cdot k$ is a positive feedback gain that can vary the input resistance, subsequently forming another degree of freedom to achieve input matching when g_m is specified for other purposes. Notably, $n \cdot k$ must be less than one to ensure the stability of CG LNA-1.

2) NF: The dominant noise current sources are assumed here to be channel thermal noise $I_{n,M1}$ of M_1 and thermal noise $I_{n,RL}$ of R_L. Fig. 3 shows the noise equivalent half circuit of CG LNA-1, where noise current source $I_{n,RS}$ is the thermal noise contributed by R_S. Also, F of CG LNA-1 under input matching is derived as

$$\begin{aligned} F &\approx 1 + F_{M1} + F_{RL} \\ &= 1 + \frac{\gamma}{\alpha} \frac{(1 - n \cdot k)}{(1 + A_{\rm neg})} + \frac{4R_S}{R_L}(1 - n \cdot k)^2 \end{aligned} \quad (5)$$

where F_{M1}, given by the second term of right-hand side in (5), is the channel thermal noise contributed by M_1; F_{RL}, given by the last term on the right-hand side of (5), is the thermal noise contributed by R_L. In contrast with (2), (5) indicates that the additional positive feedback gain $n \cdot k$ significantly suppresses both F_{M1} and F_{RL}. Obviously, both F_{M1} and F_{RL} decrease with increasing $n \cdot k$.

3) Voltage Gain and 3-dB Gain Bandwidth: The 3-dB gain bandwidth of CG LNA-1 is analyzed by considering an output half circuit of CG LNA-1, as shown in Fig. 4. In this figure, L_S acts as a series-peaking inductance. The combination of L_S, C_d,

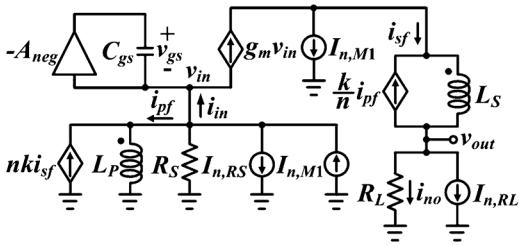

Fig. 3. Noise equivalent half circuit of the proposed CG LNA-1.

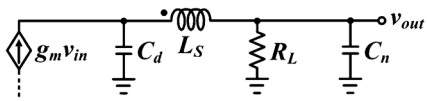

Fig. 4. Output half circuit of the proposed CG LNA-1.

and C_n forms two additional poles in the voltage-gain transfer function to subsequently extend the 3-dB gain bandwidth. The normalized transimpedance $Z_N(s)$ of CG LNA-1 is derived as

$$Z_N(s) = \frac{v_{\rm out}(s)}{g_m R_L v_{\rm in}(s)} \approx \frac{1}{1 + \frac{s}{\omega_c} + \frac{k_c}{m_{1A}}\frac{s^2}{\omega_c^2} + \frac{k_c(1-k_c)}{m_{1A}}\frac{s^3}{\omega_c^3}} \tag{6}$$

where ω_c, k_c, and m_{1A} are $1/R_L(C_d+C_n)$, $C_d/(C_d+C_n)$, and $R_L^2(C_d+C_n)/L_S(1-k^2)$, respectively. Equation (6) reveals that the bandwidth extension ratio (BWER), which refers to the ratio of 3-dB gain bandwidth with gain peaking to that without gain peaking, increases with k_c and m_{1A}. Furthermore, m_{1A} is enlarged by an increasing k, subsequently boosting BWER. Moreover, the voltage gain of CG LNA-1 can be written as

$$A_v(s) = \frac{Z_N(s) R_L}{Z_{\rm in}(s)}. \tag{7}$$

Clearly, from (6) and (7), there are three poles in the voltage-gain transfer function, which can be properly designed to increase the 3-dB gain bandwidth of CG LNA-1.

C. Differential CG LNA With a g_m-Boosted and Shunt–Shunt Dual Feedback

Fig. 5 shows a half circuit of the proposed CG LNA-2 using a g_m-boosted feedback as a shunt–shunt negative feedback and a transformer feedback as a shunt–shunt positive feedback to obtain an ultra-wide bandwidth. As illustrated in Fig. 6(a), the combined effect of the secondary winding inductance L_S of the transformer and the output equivalent π-section network forms a shunt-series peaking, causing resonances at ω_1 and ω_2 to extend the 3-dB gain bandwidth [21], as shown in Fig. 6(b). Moreover, the input matching bandwidth also increases significantly. The expressions of input impedance, NF, voltage gain, and 3-dB gain bandwidth of CG LNA-2 are derived as follows.

1) Input Impedance: Fig. 7 illustrates the small-signal equivalent half circuit of CG LNA-2, which ignores the channel length modulation of M_1. The $Z_{\rm in}(s)$ of CG LNA-2 is found as

$$Z_{\rm in}(s) = \left[g_m(1 + A_{\rm neg}) + sC_{\rm gs} + \frac{1}{sL_P} + Y_f(s) \right]^{-1} \tag{8}$$

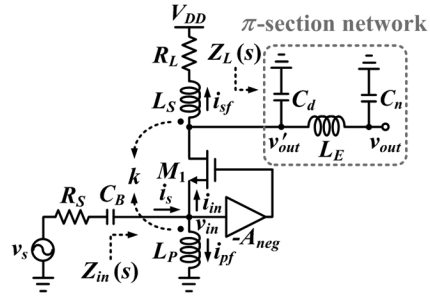

Fig. 5. Half circuit of the proposed CG LNA-2.

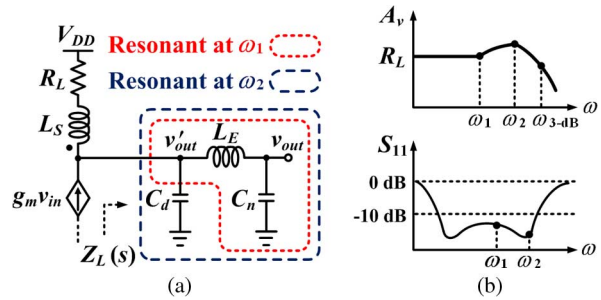

Fig. 6. (a) Output half circuit of the proposed CG LNA-2. (b) Frequency response of voltage gain and $|S_{11}|$ magnitude.

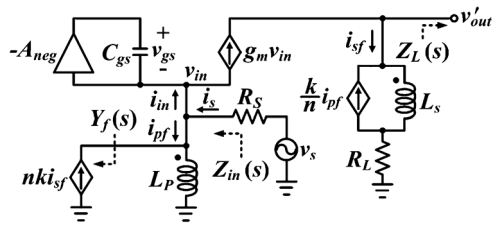

Fig. 7. Small-signal equivalent half circuit of the proposed CG LNA-2.

where

$$Y_f(s) = \frac{n \cdot k\,[n \cdot k - g_m Z_L(s)]}{Z_L(s) + R_L + sL_S(1-k^2)} \tag{9}$$

$$Z_L(s) = \frac{1}{sC_d} \| \left(sL_E + \frac{1}{sC_n} \right). \tag{10}$$

In (10), $Z_L(s)$ is the input impedance of the output π-section network that is short circuited and open circuited at ω_1 and ω_2, respectively, as shown in Fig. 6(a). The frequencies of ω_1 and ω_2 are given as

$$\omega_1 = \frac{1}{\sqrt{L_E C_n}} \tag{11}$$

$$\omega_2 = \frac{1}{\sqrt{\frac{L_E C_d C_n}{(C_d + C_n)}}}. \tag{12}$$

Consequently, the imaginary part of the feedback admittance $Y_f(s)$ shown in Fig. 8 has two zeros at ω_1 and ω_2 through the positive feedback, which thereby causes triple resonances in $Z_{\rm in}(s)$ according to (8) to broaden the input impedance bandwidth. In contrast, CG LNA-gb and CG LNA1 have a relatively narrow bandwidth because only one resonant frequency,

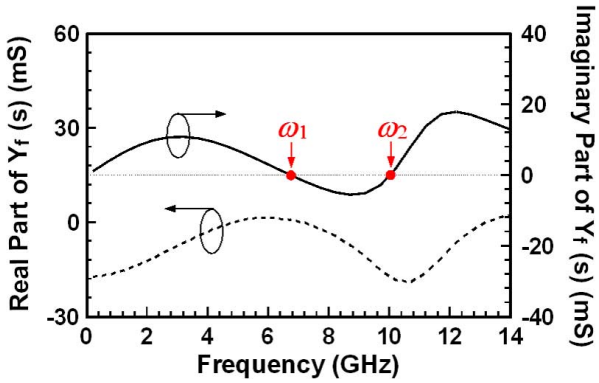

Fig. 8. Calculated real and imaginary parts of $Y_f(s)$. ($g_m = 20$ mS, $n \cdot k = 0.5$, $A_{\rm neg} = 0.9$, $C_d = 95$ fF, $C_n = 110$ fF, $L_S = 3.6$ nH, $L_E = 4.5$ nH, and $R_L = 200\ \Omega$.)

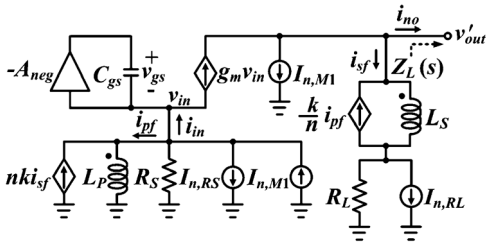

Fig. 9. Noise equivalent half circuit of the proposed CG LNA-2.

$\omega_z = 1/\sqrt{L_P C_{\rm gs}}$, is found in $Z_{\rm in}(s)$. Empirically, ω_1 and ω_2 are selected as the lower and upper bounds, respectively, of the additional bandwidth to be gained.

Incorporating (11) and (12) into (8) allows us to derive that the real part of $Z_{\rm in}(s)$ has a lower bound at ω_1 and an upper bound at ω_2, as shown by

$$\left[g_m(1+A_{\rm neg})+(n\cdot k)^2/R_L\right]^{-1}\Big|_{s=j\omega_1} \le {\rm Re}\left[Z_{\rm in}(s)\right] \le \left[g_m(1+A_{\rm neg})(1-n\cdot k)\right]^{-1}\Big|_{s=j\omega_2}. \quad (13)$$

According to (13), the real part of $Z_{\rm in}(s)$ is set between 27–107 Ω in order to achieve $|S_{11}| \le -10$ dB within the 3-dB gain bandwidth. Notably, $n \cdot k$ must be less than one to ensure the stability of CG LNA-2.

2) NF: Assume that the dominant noise current sources are channel thermal noise $I_{n,M1}$ of M_1 and thermal noise $I_{n,RL}$ of R_L. Fig. 9 illustrates the noise equivalent half circuit of CG LNA-2, where noise current source $I_{n,RS}$ is thermal noise contributed by R_S. F of CG LNA-2 is also derived as

$$\begin{aligned} F \approx & 1 + F_{M1} + F_{RL} \\ = & 1 + \frac{\gamma}{\alpha}\frac{R_S}{g_m}\left[\frac{R_L/R_S - n\cdot k(1-n\cdot k)}{R_L(1+A_{\rm neg})+n\cdot k/g_m}\right]^2 \\ & + \frac{R_S}{R_L}\left[\frac{R_L/R_S + g_m R_L(1+A_{\rm neg})(1-n\cdot k)}{nk + g_m R_L(1+A_{\rm neg})}\right]^2. \end{aligned} \quad (14)$$

Equation (14) indicates that the positive feedback gain $n \cdot k$ and negative feedback gain $A_{\rm neg}$ contribute to suppressing both F_{M1} and F_{RL}. Similar to CG LNA-1, both F_{M1} and F_{RL} decrease with increasing $n \cdot k$. However, due to the constraint of (13), the g_m and $n \cdot k$ values used for CG LNA-2 are generally less than that for CG LNA-1. Therefore, it causes that CG LNA-2 has a slightly larger average NF than CG LNA-1 within the 3-dB gain bandwidth.

3) Voltage Gain and 3-dB Gain Bandwidth: The 3-dB gain bandwidth of CG LNA-2 is analyzed by considering the output half circuit shown in Fig. 6(a). The $Z_N(s)$ of CG LNA-2 is derived as

$$Z_N(s) \approx \frac{1+s(1-k^2)/m_{1B}\omega_c}{1+\frac{s}{\omega_c}+\left(\frac{1}{m_{1B}}+\frac{1-k_c}{m_{2B}}\right)\frac{s^2}{\omega_c^2}+\frac{k_c(1-k_c)}{m_{2B}}\frac{s^3}{\omega_c^3}+\frac{1}{m_{1B}}\frac{k_c(1-k_c)}{m_{2B}}\frac{s^4}{\omega_c^4}} \quad (15)$$

where ω_c, k_c, m_{1B}, and m_{2B} are $1/R_L(C_d+C_n)$, $C_d/(C_d+C_n)$, $R_L^2(C_d+C_n)/L_S(1-k^2)$, and $R_L^2(C_d+C_n)/L_E$, respectively. In contrast with (6), (15) adds another zero and pole to extend the 3-dB bandwidth of $Z_N(s)$ more effectively. Moreover, the voltage gain range of CG LNA-2 is given by

$$\frac{Z_N(s)R_L}{Z_{\rm in}(s)}\Big|_{s=j\omega_1} \le A_v(s) \le \frac{Z_N(s)R_L}{Z_{\rm in}(s)}\Big|_{s=j\omega_2}. \quad (16)$$

Equation (16) indicates that the voltage gain of CG LNA-2 in the frequency range from ω_1 to ω_2 has a lower bound at ω_1 and an upper bound at ω_2.

D. Stability

By referring to [22], the stability of the CG LNA with multiple feedbacks can be estimated by a return ratio RR, which is defined as the minus ratio of the output currents without and with the feedbacks. According to this definition, RR for the proposed CG LNAs is derived as

$$RR = -\frac{n\cdot k(1+A_{\rm neg})g_m R_S}{1+(1+A_{\rm neg})g_m R_S}. \quad (17)$$

It is deduced in [22] that unconditional stability is achieved with $-1 < RR < 0$. Therefore, the positive feedback gain $n \cdot k$ must be less than unity to make (17) satisfy this stability criterion.

E. Design Guide and Procedure

According to the input impedance and NF expressions shown in (4) and (5) for the proposed CG LNA-1 and those in (8) and (14) for the proposed CG LNA-2, the dual-feedback parameters, g_m and $n \cdot k$, play crucial roles to achieve good input matching and low NF for the two CG LNAs. Basically, increasing g_m or $n \cdot k$ reduces the NF, while increasing g_m or decreasing $n \cdot k$ lowers the input resistance. Therefore, g_m and $n \cdot k$ should be theoretically as large as possible to suppress the NF and meanwhile achieve an input matching by maintaining a 50-Ω input resistance. However, practically, there is an upper limit for g_m and $n \cdot k$ because the former is restricted by the allowable maximum current and the latter is bound by the stability condition shown in (17).

The equations derived in this section are helpful to find design conditions for the proposed CG LNAs to achieve good

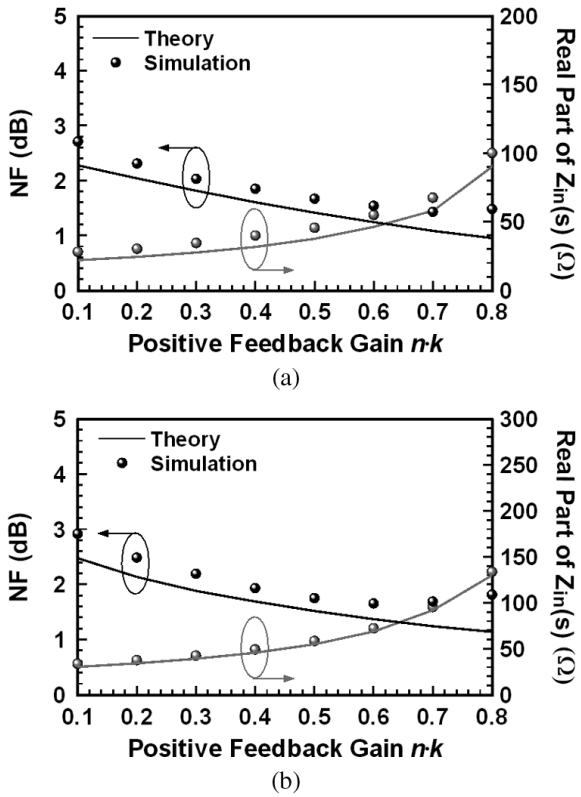

Fig. 10. Calculated NF and input resistance data using the derived equations with comparison to simulation results. (a) CG LNA-1 at 6-mA current consumption and 200-Ω load impedance. (b) CG LNA-2 at 4.1-mA current consumption and 200-Ω load impedance.

input matching and low NF at input resonance. To demonstrate the validity of the derived equations for this purpose, Fig. 10 shows the theoretical results of input resistance and NF calculated from (4), (13) and (5), (14), respectively, for the proposed CG LNAs operating under the selected bias and load conditions. The calculated data shown in Fig. 10 agree well with the simulation results. Notably, these design equations assume that the CG transistors are unilateral and the transformers are lossless.

A design procedure for the proposed CG LNAs is summarized as follows.

Step 1) Determine g_m, $n \cdot k$, and R_L using (4)–(7) for CG LNA-1 and (8)–(16) for CG LNA-2 to simultaneously achieve NF $<$ 2 dB, return loss (RL) $>$ 10 dB, and Gain $>$ 10 dB under the conditions of input resonance, unconditional stability, and allowable maximum current.

Step 2) Choose L_P to resonate with $C_{\rm gs}$ at a frequency lower than the center of the operating frequency range, and then determine L_S from the known L_P and n.

Step 3) Adjust R_L to maximize the gain-bandwidth product without violating the conditions in Step 1).

Step 4) Use the output shunt-series peaking technique, as shown in Fig. 6(a), for CG LNA-2 to extend the input impedance and 3-dB gain bandwidth to cover the entire operating frequency range.

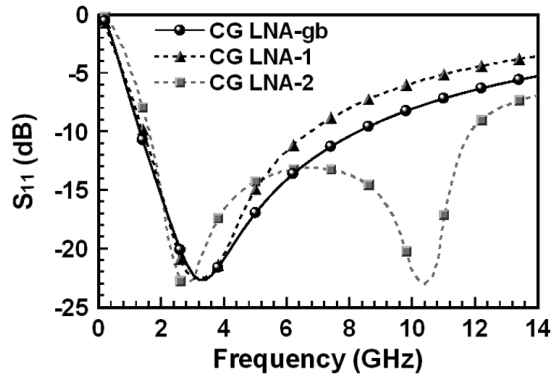

Fig. 11. Comparison of simulated magnitude of $|S_{11}|$ for the studied CG LNAs under the wideband input and noise matching condition. (Common parameters: $A_{\rm neg} = 0.9$, $L_P = 5.5$ nH; CG LNA-gb's parameters: $g_m = 15$ mS, $R_L = 260\ \Omega$; CG LNA-1's parameters: $g_m = 30$ mS, $R_L = 180\ \Omega$; $n \cdot k = 0.6$, $L_S = 5.5$ nH; CG LNA-2's parameters: $g_m = 20$ mS, $R_L = 200\ \Omega$; $n \cdot k = 0.5$, $L_S = 3.6$ nH, $L_E = 4.5$ nH.)

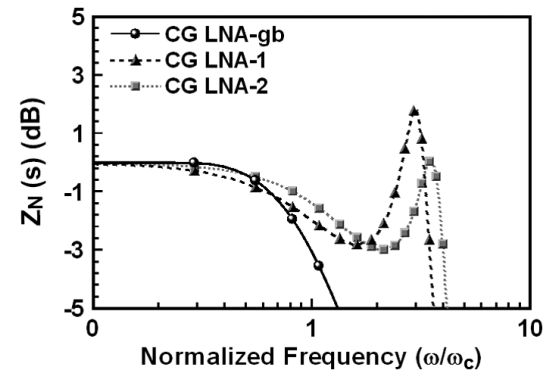

Fig. 12. Comparison of magnitude of $Z_N(s)$ for the studied CG LNAs under the wideband input and noise matching condition. (CG LNA-1 parameters: $k_c = 0.49$, $m_{1A} = 1.8$; CG LNA-2's parameters: $k_c = 0.47$, $m_{1B} = 4.1$, $m_{2B} = 3.3$.)

F. Comparison of S_{11}, BWER, and NF

Fig. 11 compares the simulated $|S_{11}|$ of the studied CG LNAs. It is found that CG LNA-2 at higher frequencies has apparently better input matching than the others. Furthermore, based on (3), (6), and (15), Fig. 12 compares the calculated $Z_N(s)$ of the CG LNAs. It is found that both CG LNA-1 and CG LNA-2 substantially increase the 3-dB gain bandwidth compared to CG LNA-gb, achieving a BWER of 3.4 and 4, respectively. Notably, if the actual transformer loss is considered, the overshoot ripples of $Z_N(s)$ for CG LNA-1 and CG LNA-2 in Fig. 12 will be smoothed over so as not to significantly affect the gain flatness.

Fig. 13 compares the simulated NF of the studied CG LNAs. Obviously, in contrast with the CG LNA-gb, both CG LNA-1 and CG LNA-2 significantly reduce NF to around 2 dB over a much wider frequency range. Despite superior capability of the CG LNA-1 having noise suppression, input mismatch occurs at higher frequencies due to the effect of the input parasitic capacitances of M_1, resulting in an inferior NF at higher frequencies. In contrast, the CG LNA-2 not only extends the 3-dB gain bandwidth, but also improves NF at higher frequencies. This

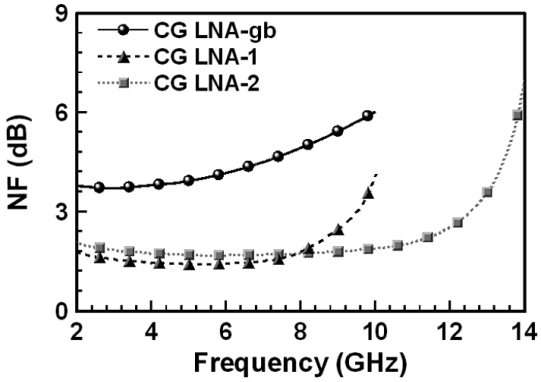

Fig. 13. Comparison of NF for the studied CG LNAs under the wideband input and noise matching condition. (The used circuit parameters are the same as those shown in the caption of Fig. 11.)

is attributed to the extension of input matching and 3-dB gain bandwidth at the same time.

III. Circuit Implementation and Results

A. Circuit Design

The theoretical predictions are verified by implementing the two proposed CMOS dual-feedback CG LNAs in a 0.18-μm 1P6M CMOS process. Figs. 14 and 15 schematically depict the circuit of CG LNA-1 and CG LNA-2, respectively, without showing bias circuits. The parasitic effects of RF pads and grounding bondwires are also considered in the design. In both dual-feedback CG LNA designs, the g_m-boosted feedback utilizes the capacitor cross-coupled (CCC) technique [23], resulting in $A_{\rm neg} \approx 0.9$ when C_G is larger than $C_{\rm gs}$. Moreover, a superior $\rm IIP_2$ is achieved using a differential amplifier configuration. Therefore, the input matching condition for both proposed CG LNAs is $Z_{\rm in,diff}(s) = 2R_S$, where $Z_{\rm in,diff}(s)$ denotes differential input impedance. Additionally, the positive feedback is constructed using a symmetric transformer with interlaced wires, as illustrated in Fig. 16(a) and (b) for use in CG LNA-1 and CG LNA-2, respectively. These transformers are mainly integrated on the top metal layer with a thickness of 2.34 μm. The magnetic coupling coefficient k of the transformers is estimated around 0.7. Therefore, the ratio n should be designed to be less than one to ensure the stability of the proposed CG LNAs. For measurement purposes, the output buffer of CG LNA-1 and CG LNA-2 consists of $M_{3A} - M_{6A}$ and $M_{3B} - M_{6B}$, respectively. More design details of both proposed CG LNAs are given as follows.

1) CG LNA-1: As shown in Fig. 14, according to (4) and (5), for simultaneously achieving $|S_{11}| \leq -10$ dB and as minimum NF as possible over the entire 3-dB gain bandwidth, the g_m value of 30 mS for both M_{1A} and M_{2A} with a gate width of 4×20 μm and an $n \cdot k$ value of about 0.6 are determined. To obtain $n \cdot k \approx 0.6$, the transformer is designed with a turn ratio $N_S : N_P = 3 : 3$ and a coupling coefficient $k = 0.65$ by selecting a metal spacing of $S_1 = 3$ μm and a metal width of $W_1 = 12$ μm, as depicted in Fig. 16(a). The extracted element quantities of the transformer from the Ansys-Ansoft HFSS electromagnetic (EM) simulation results at 8 GHz are $L_{P1} = 5.5$ nH and $L_{S1} = 5.3$ nH.

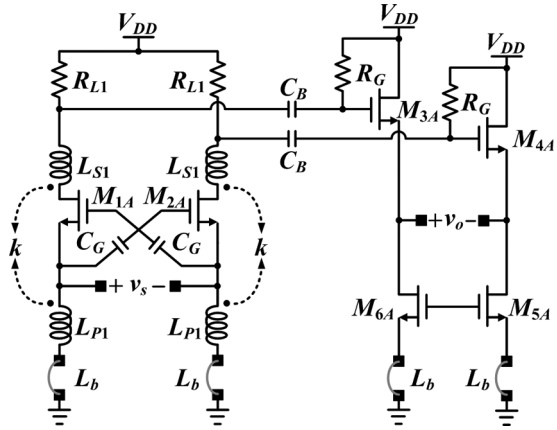

Fig. 14. Circuit schematic of CG LNA-1 with a list of device information in Table I and a bondwire inductance L_b of about 0.8 nH.

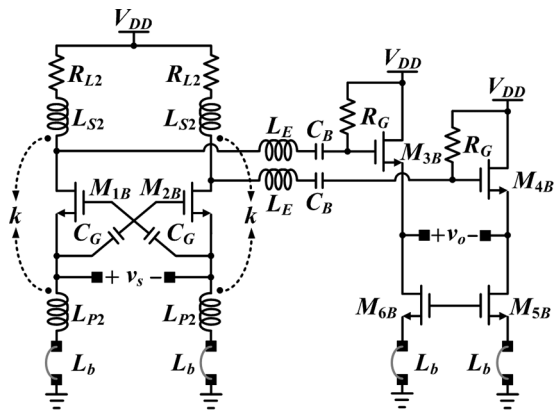

Fig. 15. Circuit schematic of CG-LNA2 with a list of device information in Table II and a bondwire inductance L_b of about 0.8 nH.

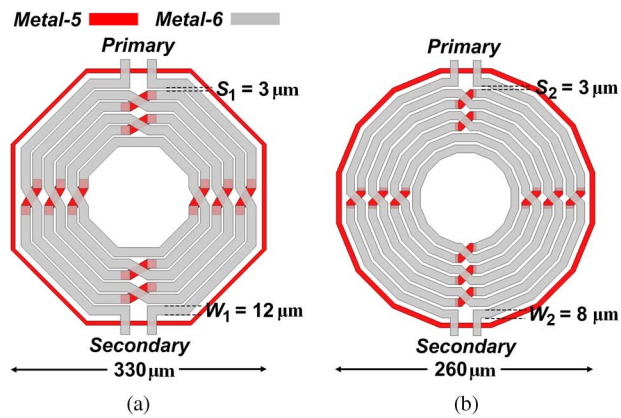

Fig. 16. Symmetric plane transformers with interlaced wires for use as a positive feedback component in the designed CG LNAs. (a) CG LNA-1. (b) CG LNA-2.

The R_{L1} value determines the voltage gain when the wideband input and noise matching has been done. The voltage gain generally increases with R_{L1}. However, the linearity issue should be addressed because a larger R_{L1} reduces the overhead voltage of M_{1A} and M_{2A}. Hence, $R_{L1} = 180\ \Omega$ is finally selected to ensure that both M_{1A} and M_{2A} are biased at saturation region, thus satisfying the high linearity requirement.

TABLE I
INFORMATION OF THE CIRCUIT ELEMENTS IN CG LNA-1

Bias current	I_{LNA}			I_{Buffer}			
Value	6 mA			4 mA			
Transistors	$M_{1A}-M_{2A}$		$M_{3A}-M_{4A}$		$M_{5A}-M_{6A}$		
W/L (μm/μm)	80 / 0.18		40 / 0.18		55 / 0.18		
Passives	R_{L1}	R_G	C_G	C_B	L_{P1}	L_{S1}	k
Value	180 Ω	3 kΩ	6 pF	4 pF	5.5 nH	5.3 nH	0.65

TABLE II
INFORMATION OF THE CIRCUIT ELEMENTS IN CG LNA-2

Bias current	I_{LNA}			I_{Buffer}				
Value	4.1 mA			3.8 mA				
Transistors	$M_{1B}-M_{2B}$		$M_{3B}-M_{4B}$		$M_{5B}-M_{6B}$			
W/L (μm/μm)	48 / 0.18		38 / 0.18		52 / 0.18			
Passives	R_{L2}	R_G	C_G	C_B	L_{P2}	L_{S2}	L_E	k
Value	200 Ω	3 kΩ	6 pF	3 pF	5 nH	3.6 nH	4.8 nH	0.65

The complete information about the circuit elements in CG LNA-1 is shown in Table I.

2) CG LNA-2: As shown in Fig. 15, according to (8) and (14), simultaneously achieving $|S_{11}| \leq -10$ dB and as minimum NF as possible over the entire 3-dB gain bandwidth involves setting the g_m value of both M_{1B} and M_{2B} with a gate width of 4×12 μm as 20 mS and an $n \cdot k$ value of about 0.5. To achieve optimum shunt-series peaking, the ratio of L_{S2} to L_E should approximate 0.75 while $k_c = 0.45$. Therefore, the transformer is designed with a turn ratio $N_S : N_P = 3 : 4$ and a coupling coefficient $k = 0.65$ to achieve minimum NF, wideband input matching, and optimum BWER simultaneously. The desired $k = 0.65$ is obtained by selecting a metal spacing of $S_2 = 3$ μm and a metal width of $W_2 = 8$ μm, as depicted in Fig. 16(b), and L_E is realized by a spiral inductor with a metal width of 8 μm. Notably, the transformer as shown in Fig. 16(b) is specially designed in a dodecagonal shape to enhance quality (Q) factor at higher frequencies. The extracted element quantities of the transformer from the Ansys-Ansoft HFSS EM simulation results at 8 GHz are $L_{P2} = 5$ nH and $L_{S2} = 3.6$ nH. Additionally, the L_E value at 8 GHz is 4.8 nH.

Similarly, the R_{L2} value determines the final voltage gain once the wideband input and noise matching has been done. Since an excessively large R_{L2} should be avoided to ensure the operation of both M_{1B} and M_{2B} in the saturation region, the R_{L2} value of 200 Ω is finally chosen to satisfy the high linearity requirement. The complete information about the circuit elements in CG LNA-2 is shown in Table II.

B. Simulated and Experimental Results

Chips for both of the proposed CG LNAs are fabricated in a 0.18-μm 1P6M CMOS process. Shielding structures have been realized on the metal–insulator–metal capacitors and RF pads to reduce the noise coupling through the substrate. Fig. 17(a) and (b) shows the chip microphotograph of CG LNA-1 and CG LNA-2, respectively. The chip area of CG LNA-1 and CG LNA-2 are 1.06 and 1.11 mm^2, respectively.

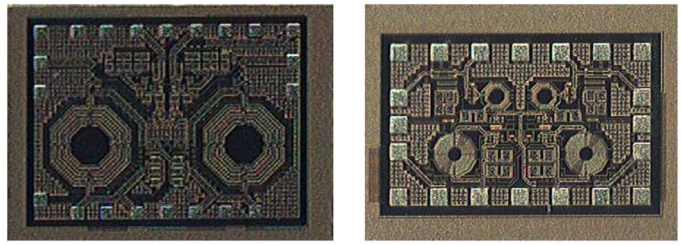

(a) (b)

Fig. 17. Chip microphotograph of the designed CG LNAs. (a) CG LNA-1. (b) CG LNA-2.

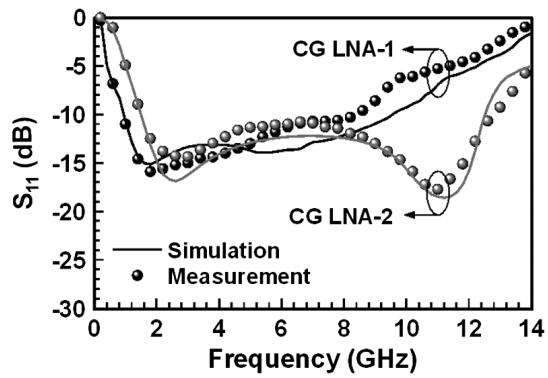

Fig. 18. Simulated and measured $|S_{11}|$ of the proposed CG LNAs.

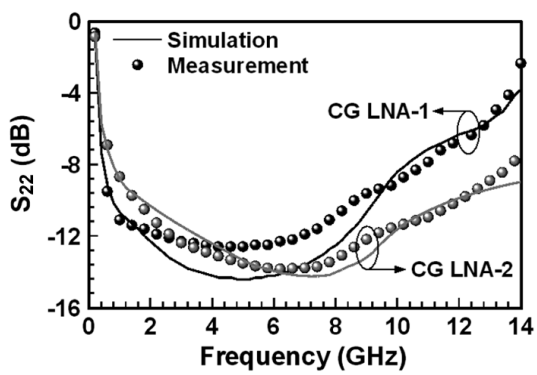

Fig. 19. Simulated and measured $|S_{22}|$ of the proposed CG LNAs.

Both chips are measured on a 0.8-mm-thick FR4 board. While operating at a supply voltage of 1.8 V, CG LNA-1 and CG LNA-2 consume dc power of 10.8 and 7.4 mW, respectively. The external wideband baluns are used to convert between single-ended and differential signals in the measurement. Notably, the loss of wideband baluns needs to be de-embedded beforehand. Fig. 18 compares the simulated and measured $|S_{11}|$ values of the two proposed dual-feedback CG LNAs. According to this figure, the measured $|S_{11}|$ less than -10 dB for CG LNA-1 is achieved over the frequency range of 1–8.4 GHz. In contrast, the measured $|S_{11}|$ of less than -10 dB for CG LNA-2 covers 1.6–12.6 GHz. Fig. 19 compares the simulated and measured $|S_{22}|$ of the two proposed CG LNAs. The measured $|S_{22}|$ is below -10 dB over the frequency range of 0.8–8 and 2–12.4 GHz for the CG LNA-1 and CG LNA-2, respectively. Fig. 20 compares the simulated and measured $|S_{12}|$ of the two proposed CG LNAs. Within

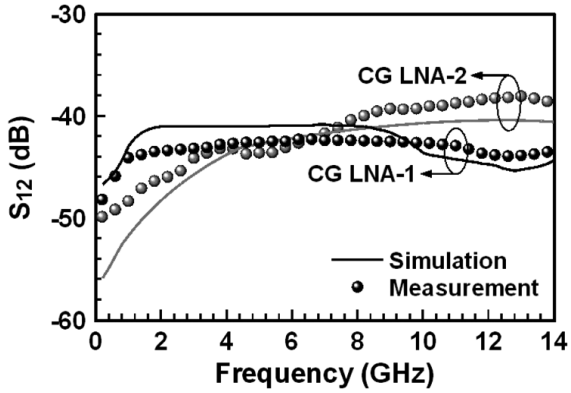

Fig. 20. Simulated and measured $|S_{12}|$ of the proposed CG LNAs.

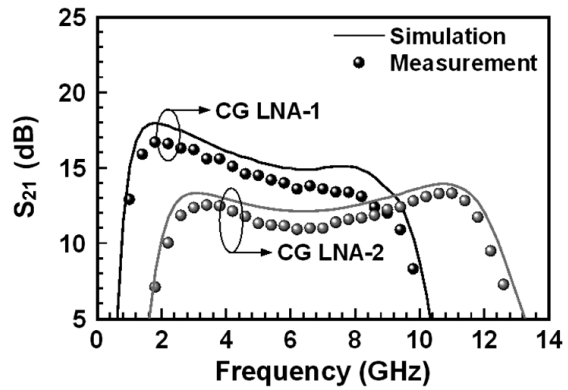

Fig. 21. Simulated and measured $|S_{21}|$ of the proposed CG LNAs.

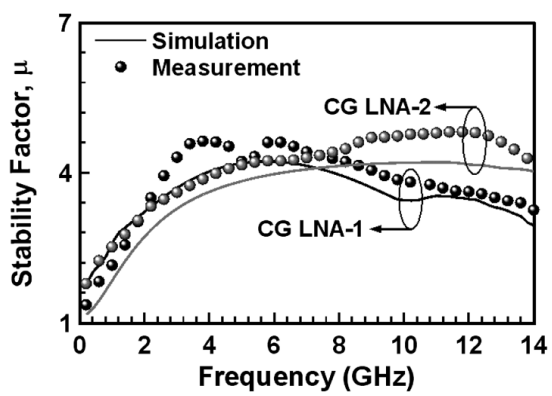

Fig. 22. Simulated and measured μ-factor of the proposed LNAs.

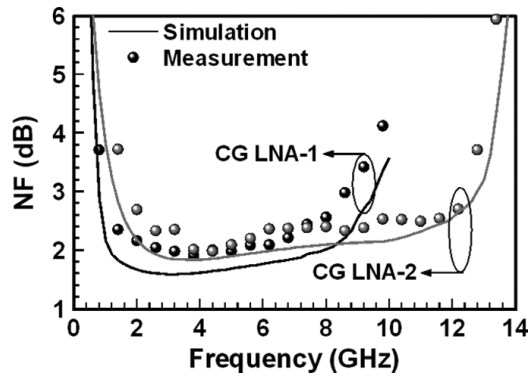

Fig. 23. Simulated and measured NF of the proposed CG LNAs.

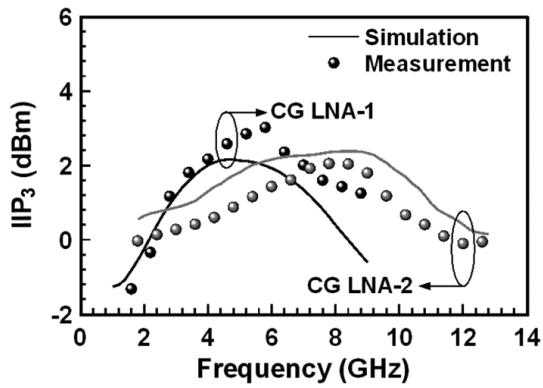

Fig. 24. Simulated and measured IIP_3 of the proposed CG LNAs.

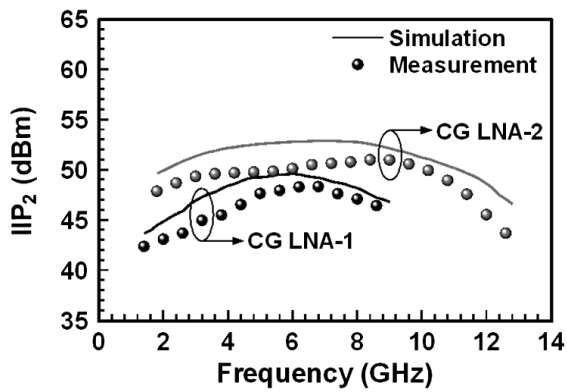

Fig. 25. Simulated and measured IIP_2 of the proposed CG LNAs.

the 10-dB impedance matching bandwidth, the measured $|S_{12}|$ results for both cases are below -35 dB.

Fig. 21 compares the simulated and measured $|S_{21}|$ of the two proposed CG LNAs. The measured $|S_{21}|$ results of CG LNA-1 and CG LNA-2 are 13.5–16.5 and 10–13 dB within the 3-dB gain bandwidth of 7 and 10 GHz, respectively. In the case of CG LNA-1, the discrepancy of $|S_{21}|$ at higher frequencies between simulated and measured results is largely due to the low Q factor of the secondary winding coil of the transformer. Additionally, the $|S_{21}|$ of CG LNA-2 is about 2.4 dB less than that of CG LNA-1 at a middle frequency around 7 GHz. This finding is expected because the voltage gain of CG LNA-2 is limited to a certain range due to the constraint of (16).

Fig. 22 shows the simulated and measured stability factor μ of the two proposed CG LNAs. This figure reveals that unconditional stability is achieved over the entire frequency range of interest. Fig. 23 shows the simulated and measured NF of the two proposed CG LNAs. The measured NF of both proposed CG LNAs is 1.9–2.6 dB within the 3-dB gain bandwidth. Clearly, CG LNA-2 has a superior NF performance at higher frequencies due to the extension of bandwidth for both input matching and 3-dB gain drop.

Figs. 24 and 25 show the simulated and measured IIP_3 and IIP_2 of the two proposed CG LNAs, respectively. The measured IIP_3 of CG LNA-1 and CG LNA-2 is -2–3 and -0.1–2.2 dBm, respectively. This finding suggests that the two proposed CG LNAs have a superior linearity because the used transformers

TABLE III
PERFORMANCE COMPARISON OF THIS WORK WITH THE STATE-OF-THE-ART WIDEBAND CMOS LNAS

Reference	$BW_{3\text{-dB}}$ (GHz)	Gain (dB)	NF (dB)	IIP_3 (dBm)	Power (mW)	FoM	CMOS (nm)	Architecture
CG LNA-1*	1 – 8	13.5 – 16.5	1.9 – 2.6	-2 – 3	10.8	5.4	180	dual feedback CG
CG LNA-2*	2.2 – 12.2	10 – 13	1.9 – 2.6	-0.1 – 2.1	7.4	7.5	180	dual feedback CG
[14]*	3.1 – 10.6	11.5 – 14.5	4.5 – 5	-4.8[b]	7	2.4	130	g_m-boosted CG
[15]*	1.3 – 12.3	5.2 – 8.2	4.6 – 5.5	7.6 – 9.1	4.5	2.4	180	g_m-boosted CG
[10]*	3.56 – 8.46	19.7 – 22.7	6 – 6.5	-9.7	34.8	0.5	90	multistage CG cascaded CS
[24]*	0.2 – 9.5	7 – 10	4.2 – 8.5[a]	-9 – -6.5	20	0.3	90	active feedback CS
[5]+	2.2 – 10.9	4.5 – 12[a]	5.27 – 7	$-2.23_{@6GHz}$	4.5	1.7	180	current-reuse CG cascoded CS
[9]+	3.1 – 10.3	9.6 – 12.7	2.5 – 3.5	-3 – 1	13.4	2	180	multistage CG cascaded CS
[11]+	1.2 – 11.9	6.7 – 9.7	4.5 – 5.1	$-6.2_{@6GHz}$	20	0.7	180	noise-canceling CG parallel CS
[13]+	0.1 – 5.2	7.7 – 10.7	2.9 – 5.4	$-6_{@1GHz}$	7	1.3	65	noise-canceling CG parallel CS
[25]+	4 – 7.8	12 – 15.6[a]	4 – 5.3	-5 – -1.2	6.4	1.5	130	CS cascoded CG

*: differential topology; +: single-ended topology
[a]: graphically estimated; [b]: frequency range unavailable

do not yield a significant voltage drop to reduce the voltage headroom of $M_{1A,(1B)}$ and $M_{2A,(2B)}$. Moreover, the measured IIP_2 of the two proposed CG LNAs averages about 46 dBm within the 3-dB gain bandwidth.

Table III summarizes the performance merits of this work with comparison to the state-of-art wideband CMOS LNAs. In this table, [24] and [25] adopt a CS input stage, while all the rest use a CG input stage. In comparison, this work has a superior NF, gain, and linearity with respect to comparable power consumption. Significantly, the proposed different dual-feedback techniques reduce the NF of CG LNAs to a minimum value of 1.9 dB. The figure-of-merit (FoM) in this table is defined by (18) [15], where gain and F are the average of maximum and minimum values within the 3-dB gain bandwidth $(\mathrm{BW}_{3\text{-dB}})$, and P_{dc} is power consumption. Obviously, the two proposed CG LNAs have superior FoM to those in previous literature,

$$\mathrm{FoM} = \frac{\mathrm{Gain[linear]} \cdot \mathrm{BW}_{3\text{-dB}}[\mathrm{GHz}]}{(F-1) \cdot P_{\mathrm{dc}}[\mathrm{mW}] \cdot 1[\mathrm{GHz}]}. \tag{18}$$

IV. CONCLUSION

This work involves designing two CMOS CG LNAs with different dual-feedback techniques to attain good input matching, low NF, and high linearity over a wide frequency range. With the dual feedback, CG LNA-1 adds a degree of freedom in the design to relieve a difficult tradeoff between input and noise matching, thus achieving a maximum gain of 16.5 dB and a minimum NF of 1.9 dB. Additionally, CG LNA-1 further uses the secondary winding coil of the transformer to perform series peaking, subsequently extending the 3-dB gain bandwidth up to 7 GHz. In contrast with CG LNA-1, CG LNA-2 remarkably extends the input matching and 3-dB gain bandwidth through a combined technique of dual shunt–shunt feedback and output shunt-series peaking. Consequently, the NF of CG LNA-2 ranges similarly from 1.9 to 2.6 dB, but over an even larger 3-dB gain bandwidth of 10 GHz.

REFERENCES

[1] V. Giannini, P. Nuzzo, C. Soens, K. Vengattaramane, M. Steyaert, J. Ryckaert, M. Goffioul, B. Debaillie, J. Van Driessche, J. Craninckx, and M. Ingels, "A 2 mm^2 0.1-to-5 GHz SDR receiver in 45 nm digital CMOS," *IEEE J. Solid-State Circuits*, vol. 44, no. 12, pp. 3486–3498, Dec. 2009.

[2] R. van de Beek, J. Bergervoet, H. Kundur, D. Leenaerts, and G. van der Weide, "A 0.6-to-10 GHz receiver front-end in 45 nm CMOS," in *IEEE Int. Solid-State Circuits Conf. Tech. Dig.*, Feb. 2008, pp. 128–129.

[3] B. G. Perumana, J.-H. Zhan, S. S. Taylor, B. R. Carlton, and J. Laskar, "Resistive-feedback CMOS low-noise amplifiers for multiband applications," *IEEE Trans. Microw. Theory Techn.*, vol. 56, no. 5, pp. 1218–1225, May 2008.

[4] M. T. Reiha and J. R. Long, "A 1.2 V reactive-feedback 3.1–10.6 GHz low-noise amplifier in 0.13 μm CMOS," *IEEE J. Solid-State Circuits*, vol. 42, no. 5, pp. 1023–1033., May 2007.

[5] R.-M. Weng, C.-Y. Liu, and P.-C. Lin, "A low-power full-band low-noise amplifier for ultra-wideband receivers," *IEEE Trans. Microw. Theory Techn.*, vol. 58, no. 8, pp. 2077–2083, Aug. 2010.

[6] J.-F. Chang and Y.-S. Lin, "0.99 mW 3–10 GHz common-gate CMOS UWB LNA using T-match input network and self-body-bias technique," *Electron. Lett.*, vol. 47, no. 11, pp. 658–659, May 2011.

[7] B. Park, S. Choi, and S. Hong, "A low-noise amplifier with tunable interference rejection for 3.1- to 10.6-GHz UWB systems," *IEEE Microw. Wireless Compon. Lett.*, vol. 20, no. 1, pp. 40–42, Jan. 2010.

[8] K.-H. Chen, J.-H. Lu, B.-J. Chen, and S.-I. Liu, "An ultra-wide-band 0.4–10-GHz LNA in 0.18-μm CMOS," *IEEE Trans. Circuits Syst. II, Exp. Briefs*, vol. 54, no. 3, pp. 217–221, Mar. 2007.

[9] Y.-T. Lo and J.-F. Kiang, "Design of wideband LNAs using parallel-to-series resonant matching network between common-gate and common-source stages," *IEEE Trans. Microw. Theory Techn.*, vol. 59, no. 9, pp. 2285–2294, Sep. 2011.

[10] D. Pepe and D. Zito, "22.7-dB gain 19.7-dBm $\mathrm{ICP}_{1\ \mathrm{dB}}$ UWB CMOS LNA," *IEEE Trans. Circuits Syst. II, Exp. Briefs*, vol. 56, no. 9, pp. 689–693, Sep. 2009.

[11] C.-F. Liao and S.-I. Liu, "A broadband noise-canceling CMOS LNA for 3.1–10.6-GHz UWB receiver," *IEEE J. Solid-State Circuits*, vol. 42, no. 2, pp. 329–339, Feb. 2007.

[12] S. C. Blaakmeer, E. A. M. Klumperink, B. Nauta, and D. M. W. Leenaerts, "Wideband balun-LNA with simultaneous output balancing, noise-canceling and distortion-canceling," *IEEE J. Solid-State Circuits*, vol. 43, no. 6, pp. 1341–1350, Jun. 2008.

[13] K.-H. Chen and S.-I. Liu, "Inductorless wideband CMOS low-noise amplifiers using noise canceling technique," *IEEE Trans. Circuits Syst. I, Reg. Papers*, vol. 59, no. 2, pp. 305–314, Feb. 2012.

[14] M. Khurram and S. M. R. Hasan, "Series peaked noise matched g_m-boosted 3.1–10.6 GHz CG CMOS differential LNA for UWB WiMedia," *Electron. Lett.*, vol. 47, no. 24, pp. 1346–1348, Nov. 2011.

[15] S. Shekhar, J. S. Walling, and D. J. Allstot, "Bandwidth extension techniques for CMOS amplifiers," *IEEE J. Solid-State Circuits*, vol. 41, no. 11, pp. 2424–2439, Nov. 2006.

[16] A. Liscidini, M. Brandolini, D. Sanzogni, and R. Castello, "A 0.13 μm CMOS front-end, for DCS1800/UMTS/802.11b-g with multiband positive feedback low-noise amplifier," *IEEE J. Solid-State Circuits*, vol. 41, no. 4, pp. 981–989, Nov. 2006.
[17] A. Liscidini, C. Ghezzi, E. Depaoli, G. Albasini, I. Bietti, and R. Castello, "Common gate transformer feedback LNA in high IIP3 current mode RF CMOS front-end," in *Proc. IEEE Custom Integr. Circuits Conf.*, Sep. 2006, pp. 25–28.
[18] S. Woo, W. Kim, C. Lee, K. Lim, and J. Laskar, "A wideband low-power CMOS LNA with positive-negative feedback for noise, gain, and linearity optimization," *IEEE Trans. Microw. Theory Techn.*, vol. 60, no. 10, pp. 3169–3178, Oct. 2012.
[19] R.-F. Ye, T.-S. Horng, and J.-M. Wu, "Wideband common-gate low noise amplifier with dual-feedback for simultaneous input and noise matching," in *IEEE Radio Freq. Integr. Circuits Symp. Dig.*, Jun. 2011, pp. 1–4.
[20] A. J. Scholten, L. F. Tiemeijer, R. Van Langevelde, R. J. Havens, A. T. A. Zegers-van Duijnhoven, and V. C. Venezia, "Noise modeling for RF CMOS circuit simulation," *IEEE Trans. Electron Devices*, vol. 50, no. 3, pp. 618–632, Mar. 2003.
[21] S. Galal and B. Razavi, "40-Gb/s amplifier and ESD protection circuit in 0.18-μm CMOS technology," *IEEE J. Solid-State Circuits*, vol. 41, no. 12, pp. 2389–2396, Dec. 2004.
[22] A. Liscidini, G. Martini, D. Mastantuono, and R. Castello, "Analysis and design of configurable LNAs in feedback common-gate topologies," *IEEE Trans. Circuits Syst. II, Exp. Briefs*, vol. 55, no. 8, pp. 733–737, Aug. 2008.
[23] W. Zhuo, X. Li, S. H. K. Embabi, J. Pineda de Gyvez, D. J. Allstot, and E. Sanchez-Sinencio, "A capacitor cross-coupled common-gate low-noise amplifier," *IEEE Trans. Circuits Syst. II, Exp. Briefs*, vol. 52, no. 12, pp. 875–879, Dec. 2005.
[24] T. Chang, J. Chen, L. A. Rigge, and J. Lin, "ESD-protected wideband CMOS LNAs using modified resistive feedback techniques with chip-on-board packaging," *IEEE Trans. Microw. Theory Techn.*, vol. 56, no. 8, pp. 1817–1826, Aug. 2008.
[25] X. Yu and N. M. Neihart, "Analysis and design of a reconfigurable multimode low-noise amplifier utilizing a multitap transformer," *IEEE Trans. Microw. Theory Techn.*, vol. 61, no. 3, pp. 1236–1246, Mar. 2013.

Rong-Fu Ye (S'11) was born in Changhua, Taiwan, on March 26, 1983. He received the B.S.E.E degree from the National Chin-Yi University of Technology, Taichung, Taiwan, in 2005, the M.S.E.E degree from the National University of Tainan, Tainan, Taiwan, in 2007, and is currently working toward the Ph.D. degree in electrical engineering at National Sun Yat-Sen University, Kaohsiung, Taiwan.

His research interests include low-power wideband CMOS receiver design and RF chip-package codesign.

Mr. Ye was the three-time recipient of the Outstanding Design Award presented by the National Chip Implementation Center, Hsinchu, Taiwan (2011–2013).

Tzyy-Sheng Horng (S'88–M'92–SM'05) was born in Taichung, Taiwan, on December 7, 1963. He received the B.S.E.E. degree from National Taiwan University, Taipei, Taiwan, in 1985, and the M.S.E.E. and Ph.D. degrees from the University of California at Los Angeles (UCLA), Los Angeles, CA, USA, in 1990 and 1992, respectively.

Since August 1992, he has been with the Department of Electrical Engineering, National Sun Yat-Sen University, Kaohsiung, Taiwan, where he was the Director of the Telecommunication Research and Development Center (2003–2008), Director of the Institute of Communications Engineering (2004–2007), and where he is currently a Distinguished Professor. He has authored or coauthored over 200 technical publications published in refereed journals and conferences proceedings, mostly in IEEE publications. He holds over ten patents. His research interests include RF and microwave integrated circuits (ICs) and components, RF signal integrity for wireless system-in-package, digitally assisted RF technologies, and green radios for cognitive sensors and Doppler radars.

Dr. Horng has served on several Technical Program Committees of international conferences including the International Association of Science and Technology for Development (IASTED) International Conference on Wireless and Optical Communications, the IEEE Region 10 International Technical Conference, the IEEE International Workshop on Electrical Design of Advanced Packaging and Systems (EDAPS), the Asia–Pacific Microwave Conference (APMC), the IEEE Radio and Wireless Symposium (RWS), and the Electronic Components and Technology Conference (ECTC). He has also served on the Project Review Board of the Programs of Communications Engineering and Microelectronics Engineering, National Science Council, Taiwan. He is the founder chair of the IEEE Microwave Theory and Techniques Society (IEEE MTT-S) Tainan Chapter. He is currently an associate editor for the IEEE TRANSACTIONS ON MICROWAVE THEORY AND TECHNIQUES. He is a member of the IEEE MTT-S Technical Committee MTT-10 and MTT-20. He was the recipient of the 1996 Young Scientist Award presented by the International Union of Radio Science, the 1998 Industry–Education Cooperation Award presented by the Ministry of Education, Taiwan, and the 2010 Distinguished Electrical Engineer Award presented by the Chinese Institute of Electrical Engineering, Kaohsiung Branch, Taiwan. He was also the recipient of the 2011 Advanced Semiconductor Engineering (ASE) Inc. Chair Professorship and the 2012 Outstanding Research Award of National Sun Yat-Sen University.

Jian-Ming Wu (S'00–M'06) was born November 13, 1974, in Kaohsiung, Taiwan. He received the B.S.E.E degree from Yuan Ze University, Chungli, Taiwan, in 1997, and the M.S.E.E. and Ph.D. degrees from the National Sun Yat-Sen University, Kaohsiung, Taiwan, in 2000 and 2006, respectively.

In August 2006, he joined the Graduate Institute of Communication Engineering, National University of Tainan, Tainan, Taiwan, as an Assistant Professor. In August 2007, he joined the Department of Electronic Engineering, National Kaohsiung Normal University, Kaohsiung, Taiwan, as an Assistant Professor, and became an Associate Professor in March 2012. His current research interests include design of monolithic microwave integrated circuits, modeling of RF components, and chip-package-board codesign.

Dr. Wu has served on the IC Implementation Review Committee, National Chip Implementation Center, Hsinchu, Taiwan, since 2006. He was the recipient of the 2006 National Sun Yat-Sen University Outstanding Doctoral Dissertation Award.